

Rotational evolution of solar-type protostars during the star-disk interaction phase

F. Gallet¹, C. Zanni², and L. Amard³

¹ Univ. Grenoble Alpes, CNRS, IPAG, 38000 Grenoble, France
e-mail: florian.gallet1@univ-grenoble-alpes.fr

² INAF – Osservatorio Astrofisico di Torino, Strada Osservatorio 20, 10025 Pino Torinese, Italy

³ University of Exeter, Department of Physics & Astronomy, Stoker Road, Devon, Exeter EX4 4QL, UK

Received 8 March 2019 / Accepted 3 October 2019

ABSTRACT

Context. The early pre-main sequence phase during which solar-mass stars are still likely surrounded by an accretion disk represents a puzzling stage of their rotational evolution. While solar-mass stars are accreting and contracting, they do not seem to spin up substantially.

Aims. It is usually assumed that the magnetospheric star-disk interaction tends to maintain the stellar rotation period constant (“disk-locking”), but this hypothesis has never been thoroughly verified. Our aim is to investigate the impact of the star-disk interaction mechanism on the stellar spin evolution during the accreting pre-main sequence phases.

Methods. We devised a model for the torques acting on the stellar envelope based on studies of stellar winds, and we developed a new prescription for the star-disk coupling founded on numerical simulations of star-disk interaction and magnetospheric ejections. We then used this torque model to follow the long-term evolution of the stellar rotation.

Results. Strong dipolar magnetic field components up to a few kG are required to extract enough angular momentum so as to keep the surface rotation rate of solar-type stars approximately constant for a few Myr. Furthermore an efficient enough spin-down torque can be provided by either one of the following: a stellar wind with a mass outflow rate corresponding to $\approx 10\%$ of the accretion rate, or a lighter stellar wind combined with a disk that is truncated around the corotation radius entering a propeller regime.

Conclusions. Magnetospheric ejections and accretion powered stellar winds play an important role in the spin evolution of solar-type stars. However, kG dipolar magnetic fields are neither uncommon or ubiquitous. Besides, it is unclear how massive stellar winds can be powered while numerical models of the propeller regime display a strong variability that has no observational confirmation. Better observational statistics and more realistic models could contribute to help lessen our calculations’ requirements.

Key words. stars: solar-type – stars: magnetic field – stars: evolution – stars: rotation – stars: winds, outflows

1. Introduction

Classical T Tauri stars (CTTS) are magnetically active pre-main sequence stars surrounded by an accretion disk (Collier Cameron & Campbell 1993; Edwards et al. 1993, 1994; Collier Cameron et al. 1995; Hartmann et al. 1998). Their magnetic field (up to a few kG, see Johns-Krull et al. 2009; Gregory et al. 2012) has a strong impact on the dynamics and the structure of the stellar environment and can lead to the truncation of the disk and accretion of material along funnel flows down to the stellar surface, the launch of stellar winds along the opened magnetic field lines (Matt & Pudritz 2005a, 2008; Matt et al. 2012, 2015; Cranmer & Saar 2011; Réville et al. 2015; Johnstone et al. 2015; See et al. 2018; Finley & Matt 2018), and the ejection of material due to the magnetic star-disk interaction (Shu et al. 1994; Ferreira et al. 2000; Romanova et al. 2009; Zanni & Ferreira 2013).

Additionally, observations suggest (see Edwards et al. 1993; Bouvier et al. 1993; Rebull et al. 2004; Irwin & Bouvier 2009) that while stars contract during the early pre-main sequence (PMS) phase (1–10 Myr) and accrete angular momentum from the disk, they do not seem to noticeably spin up for several Myr. Indeed, Gallet & Bouvier (2013; 2015, and references therein) highlight the apparent steady evolution of the three percentiles (90th, median, and 25th) of the rotational period distributions of stars from 1 Myr to 10 Myr. The fact that the two extreme

percentiles remain almost constant in time confirms that the evolution of the rotation is not random but strongly depends on the initial conditions, that is, whether the star is initially in a fast or slow rotating regime. Since this constant rotational phase is comparable to the disk lifetime, it suggests a link between the magnetic star-disk interaction and this observed behaviour. Finally, regardless of the physical origin of this rotational evolution, these observational constraints suggest that during this early-PMS phase, a large fraction of the angular momentum of the star needs to be removed.

Moreover, the magnetospheric star-disk interaction scenario is still the main paradigm to interpret the angular momentum evolution of CTTS (see Bouvier et al. 2014, for a review). The first attempts to model the star-disk angular momentum exchange in CTTS (see e.g. Königl 1991) were based on the Ghosh & Lamb (1979) model, which was originally developed for X-ray pulsars. In this framework, the star can transfer its angular momentum to the disk along magnetic field lines that connect the star with the disk region beyond the corotation radius. This scenario popularized the idea that the disk itself could adjust the stellar rotation at the observed values (disk-locking mechanism). In more recent times, the Ghosh & Lamb (1979) model has been revised (Matt & Pudritz 2005b), thus showing that this mechanism is actually very inefficient since the size of the disk region that is magnetically connected to the star is

likely very small and often confined inside the corotation radius (Zanni & Ferreira 2013). As of today, outflows emerging from the star-disk interaction region seem to be the best viable mechanism to extract the excess of stellar angular momentum. Shu et al. (1994) proposed that a wide-angle outflow that is launched from a small region located around the corotation radius, the “X-Wind”, could be able to extract a sizable fraction of the disk angular momentum at corotation before it falls onto the star, thus at least eliminating the spin-up torque due to accretion. Stellar winds, which are possibly powered by accretion (accretion powered stellar wind, hereafter APSW, see Matt & Pudritz 2005a), can directly extract angular momentum from the star. Additionally, accurate estimates of the spin-down torque have been computed via direct numerical simulations (Matt & Pudritz 2008; Matt et al. 2012; Réville et al. 2015; Pantolmos & Matt 2017; Finley & Matt 2018). Another class of outflows can exploit the stellar magnetosphere that still connects the star to the disk, causing ejections that are intrinsically unsteady and possibly quasi-periodic. If the magnetic moment of the field that threads the disk is aligned with the stellar one, a reconnection X-point forms in the disk midplane, where matter can be uplifted from the disk and accelerated by the stellar rotation along newly opened field lines, thus removing stellar angular momentum (“ReX-wind”, Ferreira et al. 2000). If the stellar and disk magnetic moments are anti-parallel, as in the case where the open disk magnetic field is a leftover of the star-disk interaction, unsteady ejections can arise due to the quasi-periodic process of inflation, opening and reconnection of the closed magnetospheric field lines (magnetospheric ejections, hereafter MEs, Romanova et al. 2009; Zanni & Ferreira 2013). Since these two last outflow types take advantage of magnetic field lines that still connect the star with the disk, they can exchange mass, energy, and angular momentum with both the star and the disk.

The works by Gallet & Bouvier (2013, 2015) and Amard et al. (2016), aimed at comparing theoretical models and observations of the rotational evolution of solar-mass stars, make the hypothesis that during the accreting T Tauri phase the stellar rotation is kept constant thanks to a “disk-locking” mechanism, but they did not take into account the actual details of any magnetospheric star-disk interaction model. The aim of this work is to add self-consistent elements to a physical model of the star-disk interaction and to the evolutionary tracks presented in Gallet & Bouvier (2013, 2015) and Amard et al. (2016) in order to determine under which physical conditions the stellar rotation period can be kept approximately constant while the protostars are still accreting and contracting. To model the stellar spin evolution we include the spin-down torque exerted by a stellar wind, employing the parametrization proposed by Matt et al. (2012). Nevertheless, we present a new prescription for the angular momentum exchange between a star and a surrounding accretion disk based on the numerical magnetohydrodynamic (MHD) simulations of Zanni & Ferreira (2013) that show the impact of MEs on the stellar angular momentum evolution. We did not consider a Ghosh & Lamb-like star-disk magnetic coupling since it has been tested to provide a rather inefficient spin-down torque (see e.g. Matt et al. 2010), and we preferred taking into account scenarios that rely on outflows. We did not consider either X-wind (Shu et al. 1994) or ReX-wind (Ferreira et al. 2000) scenarios that are still based on phenomenological models and we preferred to include mechanisms for which self-consistent MHD numerical solutions are currently available.

The structure of this article is as follows: in Sect. 2, we briefly present the angular momentum evolution model together with the different star-disk interaction processes used in this

study. The outcome of our rotational evolution models is presented in Sect. 3. In Sect. 4, we discuss the implications of these models, in particular on the magnetic field intensity and the kind of star-disk interaction regimes that could provide a torque that is efficient enough to slow down the stellar surface. We finally draw conclusions about the validity and limitations of these models in Sect. 5.

2. The model

We build upon the model described in Gallet & Bouvier (2013) that is dedicated to the study of the angular momentum evolution of solar-type stars (i.e. stars with solar mass and metallicity). In this two-zone model, the stellar convective envelope and the radiative interior are separated entities that exchange angular momentum over a given time-scale, and the stellar internal structure evolves with time. Additionally, during the stellar evolution after the accretion disk has been dissipated, a magnetized stellar-wind torque is applied to the convective region. However, no physical description of the star-disk interaction process was included and it was simply assumed that the rotational period remained constant during the disk accretion phases (“disk-locked” state).

In the present paper, we include the impact of a self-consistent star-disk interaction model, encompassing the effect of MEs and APSWs on the early PMS stellar angular momentum evolution. In the following sections, we present the main features of our angular momentum evolution model.

2.1. Rotational evolution

The temporal evolution of the surface stellar angular velocity is governed by the angular momentum evolution of the stellar convective envelope :

$$\dot{J}_{\text{conv}} = I_{\text{conv}} \dot{\Omega}_{\star} + \dot{J}_{\text{conv}} \Omega_{\star} = \Gamma_{\text{ext}} + \Gamma_{c-e} + \Gamma_{\text{rad}}, \quad (1)$$

where $J_{\text{conv}} = I_{\text{conv}} \Omega_{\star}$ is the angular momentum of the convective envelope, I_{conv} is its moment of inertia, and Ω_{\star} its angular velocity. The term Γ_{ext} is the sum of all of the external torques acting on the stellar surface, while Γ_{c-e} is the torque associated with the core-envelope angular momentum exchange and Γ_{rad} is the angular momentum variation of the convective envelope due to the development of the radiative core (see e.g. Allain 1998; Gallet & Bouvier 2015; Amard et al. 2016). We note that $\dot{J}_{\text{conv}} \Omega_{\star}$ is related to the variation of angular velocity due to the change of the moment of inertia of the convective envelope. This takes into account the stellar contraction and the growth of the core mass, whereas we have neglected the change of the moment of inertia due to mass accretion from the surrounding disk and mass loss associated with stellar outflows. In the following we refer to “internal torque” as $\Gamma_{\text{int}} = \Gamma_{c-e} + \Gamma_{\text{rad}} - \dot{J}_{\text{conv}} \Omega_{\star}$.

To compute the torque Γ_{c-e} , we follow MacGregor & Brenner (1991). It implies that both the core and the envelope are in solid body rotation with different angular velocities. A quantity ΔJ of angular momentum is then exchanged between the core and the envelope over a time-scale τ_{c-e} (hereafter the core-envelope coupling time-scale). The quantity ΔJ is the amount of angular momentum that the core and the envelope have to exchange instantaneously in order to have the same angular velocity. We also assume, as in Allain (1998), that τ_{c-e} is constant for a given model.

The “disk-locked” condition assumed in Gallet & Bouvier (2013, 2015) implies that during the accretion

phase $\dot{\Omega}_\star = (\Gamma_{\text{ext}} + \Gamma_{\text{int}})/I_{\text{conv}} = 0$, which gives $\Gamma_{\text{ext}} = -\Gamma_{\text{int}}$. Here we remove this simplifying assumption by taking into account the internal torques and providing an explicit expression for the external torques acting during the disk lifetime. These terms depend on the characteristics and the structure of the star, summarized in Sect. 2.2, and the torques associated with the magnetospheric star-disk interaction, presented in Sect. 2.3.

2.2. Stellar parameters, internal rotation, and magnetic field

To follow the evolution of the stellar structure from the PMS to the end of the MS, we used the standard solar mass model at solar metallicity $Z = 0.013446$ (Asplund et al. 2009), from the grid of Amard et al. (2019) computed with STAREVOL, with a mixing length parameter $\alpha = 1.973$ and an initial helium mass fraction Y , which is equal to 0.269. The initial time t_0 of the model is 970 yr but we only start to display the evolution at 1 Myr since there are no observations before the Orion Nebula Cluster (hereafter ONC) age. It is important to note that the structure models do not include the effects of accretion or rotation, and they evolve at a constant mass during the disk-coupling phase.

All of the external torques that are presented in Sect. 2.3 require the intensity of the dipole component of the stellar magnetic field B_{dip} as input. In Gallet & Bouvier (2013, 2015), B_{dip} was initially identified as the mean magnetic field B_{CR} estimated by the BOREAS¹ routine (Cranmer & Saar 2011) that provides the temporal evolution of the mean magnetic field intensity as a function of stellar parameters. In Cranmer & Saar (2011) the mean magnetic field B_{CR} is given by

$$B_{\text{CR}} = 1.13 \sqrt{\frac{8\pi\rho_*k_B T_{\text{eff}}}{\mu m_{\text{H}}}} \frac{0.55}{[1 + (x/0.16)^{2.3}]^{1.22}}, \quad (2)$$

where $x = Ro/Ro_\odot$ with $Ro = P_{\text{rot}}/\tau_{\text{conv}}$ the Rossby number with P_{rot} the rotation period, τ_{conv} the convective turnover timescale (see Wright et al. 2011; Oglethorpe & Garaud 2013, for more details about the convective turnover timescale), $Ro_\odot = 1.96$, ρ_* the photospheric mass density, k_B the Boltzmann's constant, T_{eff} the effective temperature, μ the mean atomic weight, and m_{H} the mass of a hydrogen atom.

The BOREAS routine reproduces reasonably well the mean magnetic field and the mass loss rate of the present day Sun ($\langle B_\odot \rangle \approx 2\text{--}7$ G and $\dot{M}_\odot \approx 2 \times 10^{-14} M_\odot \text{yr}^{-1}$). We note that for less massive stars, this formalism produces magnetic fields with smaller intensity than what is measured using spectropolarimetry (Morin et al. 2008, 2010). When extrapolated to convective T Tauri stars, this model does not provide magnetic fields consistent with the total mean stellar field intensity, but the strength produced by the BOREAS model is compatible with the dipolar components of CTTS (a few hundred Gauss²). We assume that our torque models only depend on the dipolar field intensity since, due to its slower radial decrease, the dipolar component is mainly responsible for the large-scale magnetic interactions of the star with its surroundings.

To further investigate the magnetic field strength required by the star-disk interaction processes to prevent the star from spin-

¹ <http://lasp.colorado.edu/~cranmer/Data/Mdot2011/>

² It is important to note that in our models, the B_{dip} value corresponds to the dipolar field intensity at the magnetic equator, which is the value entering the definition of the magnetic dipole moment. Spectropolarimetric observations that perform spherical harmonics decomposition of the surface stellar field, usually provide the values of the components at their magnetic pole (see e.g. Donati et al. 2011), which in the case of a dipole is twice its equatorial strength.

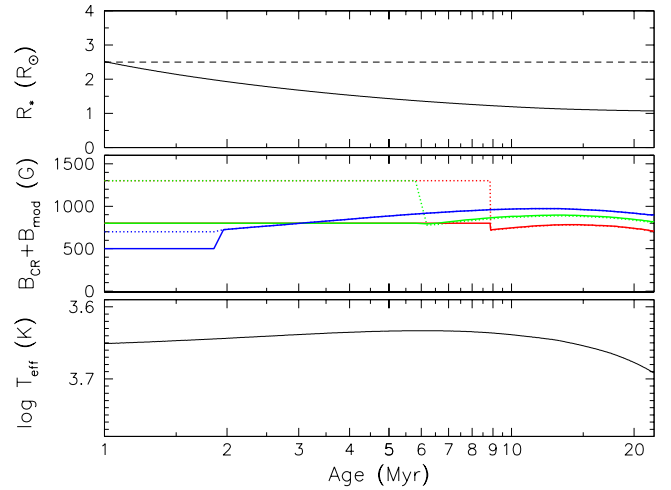


Fig. 1. Evolution of stellar radius R_\star (R_\odot) (upper panel), magnetic field $B_{\text{CR}} + B_{\text{mod}}$ (G) (middle panel), and effective temperature T_{eff} (K) (lower panel) as function of time. It is for a $1 M_\odot$ star at solar metallicity and for accretion rate at 1 Myr of $\dot{M}_{\text{acc,init}} = 10^{-9} M_\odot \text{yr}^{-1}$. The stellar model is from Amard et al. (2019). The dashed line in the upper panel corresponds to $R_\star = 2.5 R_\odot$. In the middle panel, the colours correspond to the three different initial rotation rates: fast (blue), median (green), and slow (red). The solid lines are for $Q_{\text{acc}} = 10\%$ and the dotted lines are for $Q_{\text{acc}} = 1\%$.

ning up, we introduced a dipolar magnetic field intensity B_{mod} that we assume is constant during the disk lifetime. This magnetic field strength was chosen so as to best reproduce the rotational distribution observed in the early-PMS phase. After the disk dissipation, the numerical model switches to the mean magnetic field B_{CR} , but the transition between B_{mod} and B_{CR} can be very abrupt and thus not physically consistent.

Figure 1 shows the evolution of the stellar radius (R_\star), some examples of the magnetic field intensity ($B_{\text{CR}} + B_{\text{mod}}$), and the effective temperature (T_{eff}) as a function of time. It is important to notice that the magnetic field evolution changes with the parameters that define our models, see Sect. 3. In this figure, the transition between a disk and disk-less regime is depicted by the sharp decrease of the magnetic field intensity. It corresponds to the shift between the constant required magnetic field B_{mod} to the BOREAS' magnetic field B_{CR} .

2.3. Star-disk interaction and associated torques

The star-disk interaction is described in the framework of the scenario proposed by Zanni & Ferreira (2013). The model is based on axisymmetric magnetohydrodynamic numerical simulations of the interaction of a purely dipolar magnetosphere with the surrounding accretion disk. In this context the star can exchange angular momentum with its surrounding environment in three different ways: firstly, through the accretion of angular momentum from the disk; secondly, via the action of MEs associated with the inflation, expansion, and reconnection process of closed magnetic field lines connecting the star and the disk; and thirdly with angular momentum loss due to stellar winds. Indeed, once the disk has dissipated, stellar winds remain the only spin-down torque.

2.3.1. Accretion

According to Zanni & Ferreira (2013), if the stellar magnetic field is strongly coupled to the accretion disk (i.e. assuming

that the disk material is characterized by a low enough magnetic resistivity), the stellar magnetosphere is steadily connected with the disk over a limited radial extent around the truncation radius R_t . At this radius, the accretion flow is deviated to form the accretion curtains and the star directly accretes mass and angular momentum from the disk.

We assume that the mass accretion rate evolves according to a simple decay function based on [Caratti O Garatti et al. \(2012\)](#), i.e. $\dot{M}_{\text{acc}} \propto t^{-1.2}$

$$f_{\text{decay}}(t) = \left(\frac{t_{\text{disk}}}{t_{\text{init}}} - 1 \right)^{-1.2} \left(\frac{t_{\text{disk}}}{t} - 1 \right)^{1.2}, \quad (3)$$

where t_{init} is the starting age of our simulation (i.e. 10^6 yr), t_{disk} the disk lifetime, and t the age considered. The mass accretion rate is thus defined as $\dot{M}_{\text{acc}}(t) = \dot{M}_{\text{acc,init}} f_{\text{decay}}(t)$.

We parametrize the accretion torque Γ_{acc} as

$$\Gamma_{\text{acc}} = K_{\text{acc}} \dot{M}_{\text{acc}} \sqrt{GM_{\star} R_t}, \quad (4)$$

which is proportional to the mass accretion rate \dot{M}_{acc} and to the disk specific Keplerian angular momentum in the truncation region. As it is better specified in the next section, the proportionality constant K_{acc} takes into account the fact that in the truncation region, the disk is not in Keplerian rotation because of disk outflows that have extracted a relevant fraction of the disk angular momentum. The radius R_t corresponds to the region around the star where the dipolar magnetosphere truncates the accretion disk. It can be approximated by ([Bessolaz et al. 2008](#)):

$$R_t = K_t \left(\frac{B_{\text{dip}}^4 R_{\star}^{12}}{GM_{\star} \dot{M}_{\text{acc}}^2} \right)^{1/7}, \quad (5)$$

where K_t is a dimensionless parameter. Following [Long et al. \(2005\)](#) and [Zanni & Ferreira \(2009\)](#), we assume $K_t = 0.5$.

2.3.2. Magnetospheric ejections

The MEs ([Zanni & Ferreira 2013](#)) result from the interaction of a stellar magnetosphere and an accretion disk that produces the expansion and reconnection of the magnetic field lines connecting the star with its surrounding disk. The resulting inflation at mid-latitudes of the dipolar magnetic field lines is very dynamic and goes along with outflows that can exchange mass and angular momentum with both the disk and the star. Because of the magnetic field lines reconnection, these outflows detach from the magnetosphere and continue their propagation as magnetic islands, which are disconnected from the central part of the star-disk system and are in between the open magnetic surfaces that are anchored into the star and those anchored into the disk (see Fig. 2 from [Zanni & Ferreira 2013](#)).

The opening of the magnetospheric field lines limits the size of the area over which the star and the disk are magnetically connected, which typically does not extend beyond the corotation radius:

$$R_{\text{co}} = \left(\frac{GM_{\star}}{\Omega_{\star}^2} \right)^{1/3}. \quad (6)$$

Beyond this radius, the disk and the star do not have a direct magnetic connection. Therefore, the [Ghosh & Lamb \(1979\)](#) scenario cannot be directly applied: the disk region beyond corotation, which rotates slower than the star, cannot exert any direct spin-down torque onto the star. Here, we make the assumption

that the large-scale magnetic field is responsible for the angular momentum exchange between the different parts of the system. With this approximation, angular momentum and electric currents flow along magnetic field lines. The angular momentum is deposited, or extracted, where the electric current closes perpendicularly to the field, inducing a net Lorentz force. In [Zanni & Ferreira \(2009, see Sect. 4\)](#) it is shown that in order to have an angular momentum exchange between the star and the disk region beyond the corotation radius, a magnetic connection between the two is needed. The star-disk differential rotation generates an electric current flow that closes inside the disk along these field lines, thus depositing a fraction of the stellar angular momentum. We note that the solutions presented in [Zanni & Ferreira \(2013, see Appendix A\)](#), that are used here to constrain the torque models, do not display such a large-scale star-disk magnetic connection. In these simulations, only angular momentum exchanges between the star and the stellar wind, the MEs, and the part of the disk below corotation are possible.

As it is shown in [Zanni & Ferreira \(2013\)](#), one effect of the MEs is to reduce the ‘‘Keplerian’’ accretion torque. This is qualitatively expressed by the constant $K_{\text{acc}} < 1$ that translates the fact that a fraction $1 - K_{\text{acc}}$ of the accretion torque is launched in the form of MEs. This effect is similar to the action of an X-Wind, which represents the limiting case with $K_{\text{acc}} = 0$ for which all the disk angular momentum is extracted by the wind and the disk exerts no torque onto the star. In the case of MEs, we assume a lower efficiency and employ $K_{\text{acc}} = 0.4$.

The torque directly exerted by the MEs onto the star is related to a differential rotation effect between the star and the MEs. The torque exerted by stellar magnetic field lines coupled to a region of size ΔR of the MEs can be expressed as ([Armitage & Clarke 1996; Matt & Pudritz 2005b](#))

$$\Gamma_{\text{ME}} = q \Delta R \frac{B_{\text{dip}}^2 R_{\star}^6}{R_t^4}, \quad (7)$$

where $q = B_{\phi}/B_z \propto [\Omega_{\text{MEs}} - \Omega_{\star}] / \Omega_{\text{MEs}}$ ([Livio & Pringle 1992; Armitage & Clarke 1996; Matt & Pudritz 2005a](#)) takes into account the differential rotation between the star and the MEs. This factor can be approximated as:

$$q \propto K_{\text{rot}} - \left(\frac{R_t}{R_{\text{co}}} \right)^{3/2}, \quad (8)$$

with $K_{\text{rot}} = 0.7$. A $K_{\text{rot}} < 1$ expresses the fact that the MEs rotate at a sub-Keplerian rate. Assuming $\Delta R \propto R_t$, the MEs torque can be written as:

$$\Gamma_{\text{ME}} = K_{\text{ME}} \frac{B_{\text{dip}}^2 R_{\star}^6}{R_t^3} \left[K_{\text{rot}} - \left(\frac{R_t}{R_{\text{co}}} \right)^{3/2} \right], \quad (9)$$

where $K_{\text{ME}} = 0.21$. It is interesting to note that this torque spins-down the star only for $R_t > K_{\text{rot}}^{2/3} R_{\text{co}}$ while for a lower truncation radius, the MEs spin the stellar surface up.

We used the results of the simulations presented in [Zanni & Ferreira \(2013\)](#) to calibrate the constants appearing in Eqs. (4) and (9). These results explore only a small fraction of the parameter space of the star-disk interaction problem and even this limited sample suggests that the K_{acc} , K_{rot} , and K_{ME} values are not constant and are a function of the parameters of the model, such as the mass accretion rate. However, the simple formulation adopted in this paper allows one to reproduce the main feature of the MEs scenario, such as the decrease of the accretion torque and spin-up and spin-down change depending on the relative position of the truncation and corotation radii.

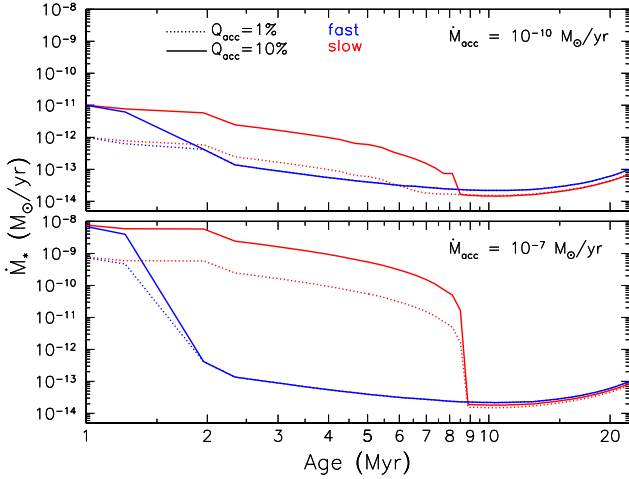


Fig. 2. Evolution of \dot{M}_* as function of time in case of fast (blue) and slow (red) initially rotating stars. For each rotators, two initial mass accretion rates are investigated $\dot{M}_{\text{acc}} = 10^{-10}$ (upper panel) and 10^{-7} (lower panel) $M_{\odot} \text{ yr}^{-1}$ with $Q_{\text{acc}} = 1$ (dotted) and 10% (solid).

2.3.3. Stellar winds

The torque exerted by the magnetized stellar winds on the stellar surface can be expressed as (see [Weber & Davis 1967](#))

$$\Gamma_{\text{wind}} = \dot{M}_{\text{wind}} r_A^2 \Omega_{\star} \quad (10)$$

where \dot{M}_{wind} is the wind mass loss rate and r_A is the average value of the Alfvén radius. We use the expression obtained by [Matt et al. \(2012\)](#)

$$r_A = K_1 \left[\frac{B_p^2 R_{\star}^2}{\dot{M}_{\text{wind}} \sqrt{K_2^2 v_{\text{esc}}^2 + \Omega_{\star}^2 R_{\star}^2}} \right]^m R_{\star}, \quad (11)$$

where $v_{\text{esc}} = \sqrt{2GM_{\star}/R_{\star}}$ is the escape velocity. We assume the values $m = 0.2177$ and $K_2 = 0.0506$, provided by [Matt et al. \(2012\)](#). The constant K_1 is given in Table 2.

In agreement with the APSW scenario ([Matt & Pudritz 2005a](#)), we assume that during the disk-accretion phase, the stellar wind takes its driving power from a fraction of the energy dissipated by the impact of the accretion columns onto the stellar surface. This establishes a relation between the accretion and the wind driving power and consequently between the mass accretion and the wind outflow rate. We take into account two values for the accretion ratio $\dot{M}_{\text{wind}}/\dot{M}_{\text{acc}} = Q_{\text{acc}} = 1\%$ and 10% ³.

After the disk has dissipated ($t > \tau_{\text{disk}}$), the stellar wind can not derive its power from accretion anymore and the stellar wind torque becomes the only spin-down mechanism left. As in [Gallet & Bouvier \(2013, 2015\)](#), during this phase the mass-loss is estimated using the BOREAS routine ([Cranmer & Saar 2011](#)) that uses the stellar angular velocity, luminosity, and radius as input. In order to prevent a sharp transition at $t = \tau_{\text{disk}}$ during the star-disk interaction regime, we use the wind mass loss rate as the maximum value between the accretion-powered and the BOREAS's rates. Figure 2 displays the evolution of the mass loss rate as a function of time from the disk accretion phase up to the late PMS for some of our models. The figure clearly shows the transition between the APSW mass loss rate and the BOREAS's mass loss rate at $t = \tau_{\text{disk}}$.

³ This assumption is equivalent to assume a $K_1 = 1.3$ constant, as originally found by [Matt et al. \(2012\)](#), and $Q_{\text{acc}} \approx 3\%$ and $Q_{\text{acc}} \approx 30\%$, respectively.

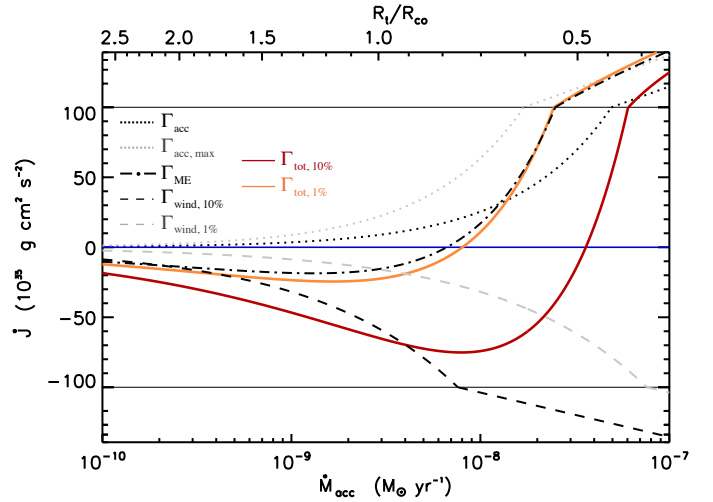


Fig. 3. External torques as function of mass accretion rate (lower axis) and corresponding truncation radius (upper axis) for given set of stellar parameters at 1 Myr ($M_{\star} = 1.0 M_{\odot}$, $R_{\star} = 2.5 R_{\odot}$, $P_{\star} = 7$ days, $B_p = 1$ kG). The accretion torque Γ_{acc} (black dotted line), the maximum spin-up torque allowed $\Gamma_{\text{acc}} (K_{\text{acc}} = 1)$ (grey dotted line), the MEs torque Γ_{ME} (dot-dashed line), the stellar wind torque Γ_{wind} for $Q_{\text{acc}} = 1\%$ (grey dashed line) and $Q_{\text{acc}} = 10\%$ (black dashed line), and the total external torque $\Gamma_{\text{ext}} = \Gamma_{\text{acc}} + \Gamma_{\text{ME}} + \Gamma_{\text{wind}}$ for $Q_{\text{acc}} = 1\%$ (orange solid line) and $Q_{\text{acc}} = 10\%$ (red solid line) are plotted.

2.3.4. External torque summary

In order to point out some important properties of the total external torque $\Gamma_{\text{ext}} = \Gamma_{\text{acc}} + \Gamma_{\text{ME}} + \Gamma_{\text{wind}}$ that acts during the accretion phases, we plot in Fig. 3 the torques presented in Sects. 2.3.1–2.3.3 as a function of the mass accretion rate for a solar mass star with a radius $R_{\star} = 2.5 R_{\odot}$, a rotation period of seven days (i.e. ≈ 0.07 of the break-up speed), and a dipolar field $B_p = 1$ kG. The black and grey dotted lines are the accretion torque and the maximum accretion torque (i.e. $K_{\text{acc}} = 1$), respectively. The torque associated to the MEs is shown with a black dot-dashed line, and the grey and black dashed line represent the stellar wind torque for $Q_{\text{acc}} = 1\%$ and $Q_{\text{acc}} = 10\%$, respectively. Finally, the orange and red solid lines show the evolution of the total external torque for $Q_{\text{acc}} = 1\%$ and $Q_{\text{acc}} = 10\%$, respectively.

As the disk truncation gets closer to the stellar surface, Γ_{ext} assumes positive values (i.e. it exerts a spin-up torque) and asymptotically approaches the limiting value $\Gamma_{\text{ext}} \approx \dot{M}_{\text{acc}} \sqrt{GM_{\star} R_t}$ (i.e. Γ_{acc} with $K_{\text{acc}} = 1$). This coincides with the fact that, in such a situation, the external torque is dominated by accretion and the spin-down effects associated with MEs become negligible ([Zanni & Ferreira 2013](#)). In this regime, even a massive stellar wind ($Q_{\text{acc}} = 10\%$) is not able to balance the accretion torque. One can notice that, in contrast with the [Zanni & Ferreira \(2013\)](#) simulations, in this regime the spin-up torque associated to the MEs is even larger than the spin-up torque due to accretion. This is a consequence of having assumed constant K_{ME} and K_{acc} values, while the [Zanni & Ferreira \(2013\)](#) simulations suggest that K_{acc} (K_{ME}) increases (decreases) with the accretion rate and the R_t/R_{co} value. On the other hand, the $\Gamma_{\text{acc}} + \Gamma_{\text{ME}}$ sum becomes comparable to the maximum total spin-up torque (Γ_{acc} with $K_{\text{acc}} = 1$), which is consistent with the simulations employed to calibrate our models.

For $Q_{\text{acc}} = 1\%$, the spin-down torque due to MEs becomes comparable to the stellar wind's torque for $R_t/R_{\text{co}} \approx 1$ and becomes more important for larger R_t/R_{co} values. For $Q_{\text{acc}} = 10\%$, the MEs and stellar wind spin-down torques become

comparable for even larger R_t/R_{co} values, corresponding to a strong propeller regime (Illarionov & Sunyaev 1975) in which the stellar centrifugal barrier prevents the disk from accreting (see Sect. 4.2). For $Q_{acc} = 1\%$, and even more so for $Q_{acc} = 10\%$, in a steadily accreting regime (i.e. $R_t < R_{co}$), the spin-down torque that is due to stellar winds is always more important than the MEs' torque.

In agreement with the Zanni & Ferreira (2013) results, the $\Gamma_{ext} = 0$ condition (i.e. when the spin-down torques associated with the MEs and the stellar wind exactly balance the accretion torque) is already attained for $R_t < R_{co}$ even in the presence of a weak stellar wind ($Q_{acc} = 1\%$). This condition is clearly not sufficient to keep the stellar angular velocity constant, which requires the spin-down torques to balance both accretion and internal torques ($\Gamma_{int} \neq 0$). For both values of Q_{acc} , it is possible to define an optimal configuration, corresponding to the minimum of the Γ_{ext} curves, as something that is related to the most efficient spin-down torque that can be obtained for a given set of stellar parameters. For $Q_{acc} = 10\%$, such a configuration is obtained for $R_t \leq R_{co}$ and the spin-down torque is dominated by the stellar wind. For $Q_{acc} = 1\%$, the maximum spin-down is attained for $R_t \geq R_{co}$ and the MEs spin-down torque becomes more important than the stellar wind torque. This is consistent with the Zanni & Ferreira (2013) results, which show that the system must enter a propeller regime in order for the star-disk interaction's spin-down torque to be strong enough to balance the stellar contraction.

As the truncation radius moves further out due to the decrease of the accretion rate, the total external torque still leads to a spin-down, but it gets weaker. For a given value of the stellar magnetic field, the increase of the differential rotation between the star and the MEs in Eq. (9) does not balance the weakening of the magnetic field intensity in the truncation region, while the stellar wind torque weakens since its mass outflow rate decreases.

3. Results

In order to compare with the observed distributions of stellar periods of rotation, we computed rotational evolution models by varying the initial (at 1 Myr) period of rotation, accretion rate, dipolar field intensity, and stellar wind mass-loss rate.

3.1. Rotational period constraints and models

We used the rotation period distribution of five star-forming regions from 1.5 Myr (The Orion Nebula Cluster, Rodríguez-Ledesma et al. 2009) to 13 Myr (the hPER cluster, Moraux et al. 2013) as observational constraints for the angular velocity evolution of solar-like stars. The age and the references for each cluster are listed in Table 1. Among these clusters, ONC, NGC 6530, Cep OB3B, and NGC 2362 display near-infrared excesses that are associated to the presence of circumstellar disks and by extension to a disk-coupling phase (Bell et al. 2013).

We computed models for slow, median, and fast rotators, which are characterized by a different initial period of rotation at 1 Myr. The initial rotation periods were chosen following Gallet & Bouvier (2015) so as to be able to compare the rotational tracks of this paper with the ones from their work. The different types of rotators are characterized by a core-envelope coupling time-scale τ_{c-e} , a disk lifetime τ_{disk} , and an initial rotational period P_{init} (see Table 2). We computed the evolution of each rotator for four different initial mass accretion rates in the range $\dot{M}_{init} = 10^{-10} - 10^{-7} M_{\odot} \text{ yr}^{-1}$ and used two possible values

Table 1. Open clusters whose rotational distributions are used in this study.

Cluster	Age (Myr)	Ref.
ONC	1.5	1
NGC 6530	2	2
Cep OB3b	4	3
NGC 2362	5	4
hPER	13	5

References. (1) Rodríguez-Ledesma et al. (2009); (2) Henderson & Stassun (2012); (3) Littlefair et al. (2010); (4) Irwin et al. (2008); (5) Moraux et al. (2013).

Table 2. Model parameters.

Parameter	Slow	Median	Fast
P_{init} (days)	8	5	1.4
τ_{c-e} (Myr)	30	28	10
τ_{disk} (Myr)	9	6	2
K_1	1.7	1.7	1.7

of the stellar wind mass loss and accretion rate ratio during the accretion phases, $Q_{acc} = 1\%$ and 10% . After the disk dissipates, the wind mass loss rate that is provided by the BOREAS model (Cranmer & Saar 2011) is employed, as in Gallet & Bouvier (2013, 2015), see Fig. 2.

During the disk accretion phases, the following two prescriptions were adopted for the dipolar field strength: firstly, B_{CR} (the Cranmer & Saar 2011 magnetic field) as provided by the BOREAS model; and secondly, B_{mod} , a constant value chosen to better reproduce the observed rotational distributions. The B_{mod} value was chosen so that the rotational tracks fit the initial stellar period at 1 Myr and the corresponding percentile of the hPER cluster at 13 Myr. Clusters older than the hPER cluster are thus not used to constrain B_{mod} . It is important to notice that we do not try to reproduce a perfectly constant spin evolution, but we follow the general assumption that a star in a given rotation state (fast/median/slow) remains in that regime from the early-PMS up to the early-MS phase. The underlying hypothesis is that the initial conditions dictate the evolution of the surface rotation rate of the stars during these phases. We recall that a constant B_{mod} is only used during the star-disk interaction phase and in both cases the Cranmer & Saar (2011) magnetic field is used to follow the angular velocity evolution after the end of the disk lifetime. The values of B_{CR} at 1 Myr, its maximum value reached during the disk lifetime, and B_{mod} are given in Table 3.

Figures 4 and 5 display the surface angular velocity evolution of fast and slow initially rotating stars as a function of age for two different accretion rates $\dot{M}_{acc,init} = 10^{-9} M_{\odot} \text{ yr}^{-1}$ and $10^{-8} M_{\odot} \text{ yr}^{-1}$, respectively. In these figures, we compare the angular velocity evolution resulting from using the MEs and APSW processes at the two Q_{acc} efficiency, either by using the Cranmer & Saar (2011) magnetic field B_{CR} (blue and red line) or the imposed magnetic field B_{mod} . It is important to note that we only display the first 20 Myr of the evolution because it is at the core of the present work.

In these figures, it is clear that for the initially slow rotating stars, the MEs and APSW processes with the imposed magnetic field B_{mod} better match the early-PMS observation than the models using the Cranmer's magnetic field. For these slow rotators,

Table 3. Magnetic field strength (in G) employed in angular velocity evolution models at 1 Myr.

(a) $Q_{\text{acc}} = 1\%$	B_{CR}			B_{mod}		
	$\dot{M}_{\text{acc}}/P_{\text{rot}}$ (d)	1.4	5	8	1.4	5
$10^{-7} M_{\odot} \text{ yr}^{-1}$	653	898	939	500	2000	2600
$10^{-8} M_{\odot} \text{ yr}^{-1}$	712	880	914	400	1200	1600
$10^{-9} M_{\odot} \text{ yr}^{-1}$	715	882	902	700	1300	1300
$10^{-10} M_{\odot} \text{ yr}^{-1}$	655	895	925	1700	2400	2200
(b) $Q_{\text{acc}} = 10\%$	B_{CR}			B_{mod}		
	$\dot{M}_{\text{acc}}/P_{\text{rot}}$ (d)	1.4	5	8	1.4	5
$10^{-7} M_{\odot} \text{ yr}^{-1}$	640	821	850	300	900	1300
$10^{-8} M_{\odot} \text{ yr}^{-1}$	699	775	785	300	600	900
$10^{-9} M_{\odot} \text{ yr}^{-1}$	715	839	821	500	800	800
$10^{-10} M_{\odot} \text{ yr}^{-1}$	655	890	911	1300	1800	1600

Notes. The values for B_{CR} , are the maximum magnetic field intensity reached by B_{CR} during the disk lifetime. The initial values (i.e. at 1 Myr) for B_{CR} are: 590, 530, 440 G for the fast, median, and slow rotators, respectively.

it suggests that a stronger magnetic field, of the order of the kG, is already required at early ages <1 Myr. However, for the initially fast rotating stars, it seems that both B_{mod} and B_{CR} are quite close to each other. It suggests that the Cranmer’s magnetic field is in that case well suited to be used in the framework of the MEs and APSW processes. However, the rotational evolution of these rotators clearly overestimates the 90th percentile of ONC, Cep OB3b, and NGC 2326. This issue was already present in Gallet & Bouvier (2013, 2015) and comes from the constraints imposed by the hPER cluster at 13 Myr. Indeed, the contraction rate and the associated increase of the surface rotation due to angular momentum conservation impose a certain initial rotation period that is not compatible with the observed percentile of the rotation distribution in the previously mentioned clusters. We note that it is not an issue linked to the completeness of the rotation period observations; the rotational distribution of Cep OBS3b does indeed seem to be fully recovered for periods <7 days (see Littlefair et al. 2010) while the completeness of NGC 2362 is close to 100% (see Irwin et al. 2008). Additionally, we can see that the free contraction matches the upper part of some of the observations. These stars are more presumably outliers, with initial conditions associated to a very short disk lifetime (<1 Myr), that therefore populate the fast rotating part of the distributions at ZAMS.

3.2. Dipolar field intensity

In Table 3 we display the dipolar magnetic field values used to compute our models, the B_{CR} value provided by the Cranmer & Saar (2011) model at 1 Myr, its maximum value during the disk lifetime, and the B_{mod} stay constant during the star-disk interaction phases so as to fit the evolutionary tracks at 1 Myr and 13 Myr.

We note that B_{CR} is comparable, at least initially, to B_{mod} , yielding an approximately constant envelope rotation during the accretion phases for fast rotator models with weaker stellar winds ($Q_{\text{acc}} = 1\%$) and accretion rates larger than $10^{-9} M_{\odot} \text{ yr}^{-1}$. See, for example, the evolutionary track in Fig. 5 for a fast rotator with $Q_{\text{acc}} = 1\%$. For fast rotator cases with a larger stellar wind mass-loss rate ($Q_{\text{acc}} = 10\%$), B_{CR} can be even larger than the “optimal” B_{mod} value, corresponding to a rapid spin-down

during the star-disk interaction stages, see for example the fast rotator model plotted with a grey line in Fig. 5.

In all other cases B_{mod} is larger than the B_{CR} estimate, with values that systematically exceed 500 G (corresponding to 1 kG maximum dipolar intensity at the magnetic pole) up to more than 2 kG (4 kG at the magnetic pole). Looking at the behaviour of the dipolar field intensity B_{mod} as a function of the free parameters of the rotational models, it is possible to highlight some trends. Given the same mass accretion rate and rotation period, the $Q_{\text{acc}} = 10\%$ models require a weaker field than the $Q_{\text{acc}} = 1\%$ cases; a more massive wind clearly provides a more efficient spin-down torque and requires a weaker magnetic field. For a fixed accretion rate, median and slow rotators require a stronger dipolar magnetic component than fast rotator; a more efficient spin-down torque is required to prevent them from spinning-up. For a given rotation period, B_{mod} displays a more complex behaviour as a function of the accretion rate, often passing through a minimum at intermediate accretion rates. This minimum of the dipolar field strength corresponds to the condition of maximum spin-down efficiency characterizing our external torque model outlined in Sect. 2.3.4 (see Fig. 3). To confirm this result, we plot in Fig. 6 the contribution of the different torques as a function of time in the case of the median rotator model for the four values of $\dot{M}_{\text{acc,init}}$ considered and for $Q_{\text{acc}} = 1\%$. In the same plots we also show the $R_{\text{I}}/R_{\text{co}}$ ratio as a function of time. The lower left panel corresponds to the minimum field intensity found in the median rotator column in Table 3a. As consistent with the torque model discussed in Sect. 2.3.4, the star-disk system transits here through a configuration characterized by $R_{\text{I}}/R_{\text{co}} \approx 1$, roughly corresponding to the minimum (i.e. maximum spin-down efficiency) of the orange solid line in Fig. 3. Similar to the discussion in Sect. 2.3.4, for a higher mass accretion rate (a lower $R_{\text{I}}/R_{\text{co}}$ ratio) the spin-down torque is dominated by the stellar wind. For a lower accretion rate, the MEs provide the main spin-down torque, while, correspondingly, the $R_{\text{I}}/R_{\text{co}}$ value becomes quite large (up to 5 for $\dot{M}_{\text{acc,ini}} = 10^{-10} M_{\odot} \text{ yr}^{-1}$). This indicates that the system is most likely in a (strong) propeller regime. Figure 6 also shows that the total torque is not constant and null in time, which would correspond to a perfect constant Ω_{\star} condition. This clearly points to the fact that the star-disk system can go through spin-down and spin-up phases during its evolution.

4. Discussion

In the Sect. 3, we show how our modelling allows us to put some constraints on the intensity of the dipolar component of the stellar magnetic field necessary to prevent the star from spinning up during the star-disk interaction phases. Here, we discuss these results, their implications for the star-disk interaction regimes that provide an efficient enough spin-down torque, and the observational constraints and biases that could support or refute our findings.

4.1. A magnetic dipole strength issue

The results presented in Sect. 3 show that, particularly in the case of median and slow rotators, dipolar magnetic fields that are stronger than 1 kG at their magnetic pole are required to efficiently reduce the stellar spin-up, independently of the main spin-down mechanism and the initial disk accretion rate. We recall that our models take into account only two specific mechanisms that can influence the stellar rotational evolution, namely stellar winds and magnetospheric ejections. However, the

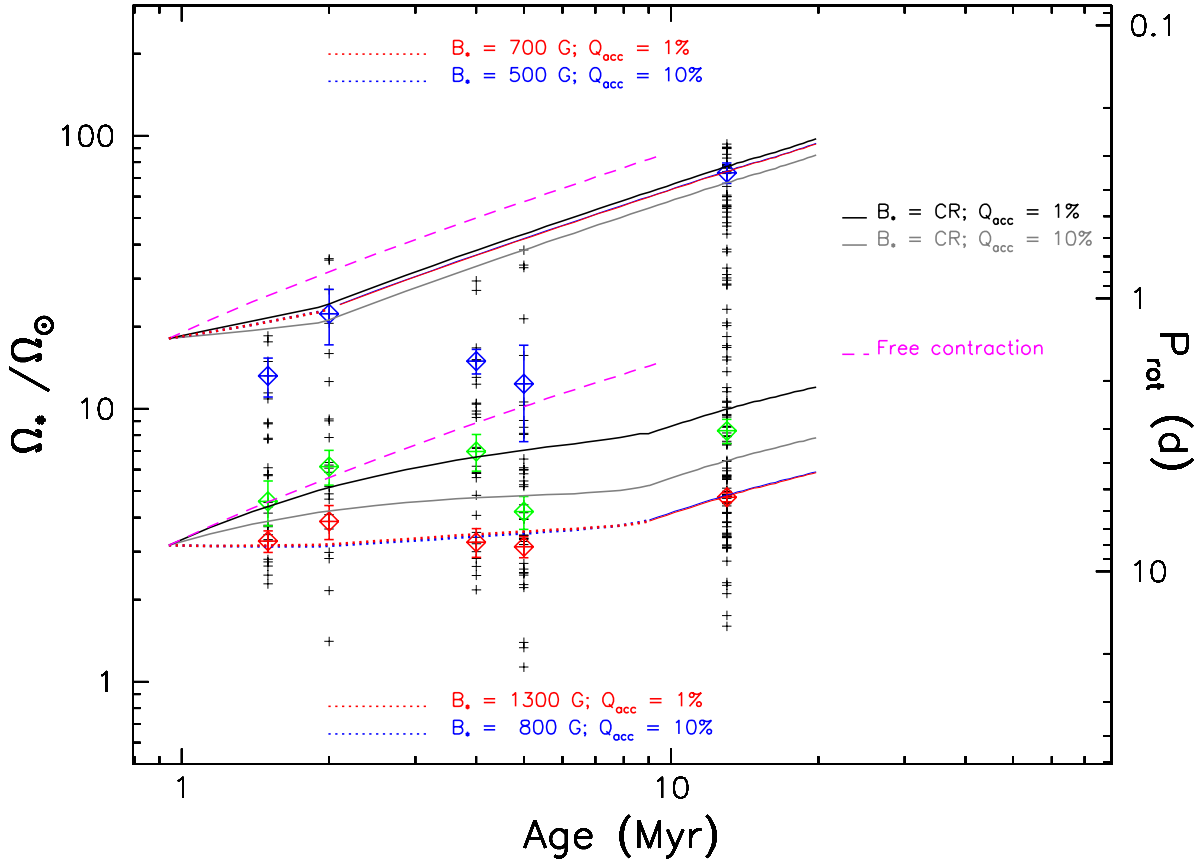


Fig. 4. Angular velocity evolution of stellar convective envelope as function of time for fast (up) and slow (down) rotator models in case where $\dot{M}_{\text{acc,init}} = 10^{-9} M_\odot \text{ yr}^{-1}$. The black and the grey solid lines represent the MEs and APSW processes with $Q_{\text{acc}} = 1\%$ and $Q_{\text{acc}} = 10\%$, respectively, and the magnetic field is from the BOREAS routine from Crammer & Saar (2011). The red and the blue dotted lines represent the models including the MEs and APSW processes with $Q_{\text{acc}} = 1\%$ and $Q_{\text{acc}} = 10\%$, respectively, but with the numerically imposed magnetic field B_{mod} . The free contraction (i.e. without any external interaction) is shown by the magenta long-dashed line. It represents the increase of the rotation rate during a free contraction phase. The angular velocity is scaled to the angular velocity of the present Sun. The blue and the red tilted square and associated error bars represent, respectively, the 90th percentile and the 25th percentile of the rotational distributions of solar-type stars in star-forming regions and young open clusters obtained with a rejection sampling method described in Gallet & Bouvier (2013).

magnetic field values that we found are consistent with the magnetic field strength found by Matt et al. (2010) who use a model similar to Ghosh & Lamb (1979). As already mentioned in Sect. 1, other possible spin-down scenarios, such as X-winds (Shu et al. 1994) or ReX-winds (Ferreira et al. 2000) were not taken into account due to the lack of a self-consistent model or torque parametrization.

Classical T Tauri stars are known to have very strong surface average magnetic fields up to a few kG (Johns-Krull 2007). Spectropolarimetric observations using the Zeeman–Doppler Imaging (ZDI) technique can also provide constraints on the topology of the stellar field, and they often indicate the presence of a complex field where the dipolar component is not always dominant (see e.g. Johnstone et al. 2014). These reconstructions need a dense and regular sample of rotation period and cold stars. One strong limitation of this technique is that depending on the structure of the magnetic field, some components can cancel each other out (Morin et al. 2010), reducing the strength of the magnetic components. Moreover, the reconstructions are done at a specific time t , neglecting the possible temporal evolution of the magnetic topology.

Keeping this in mind, we tried to apply our simple torque model presented in Sect. 2 to the sample presented in Johnstone et al. (2014), and summarized here in Table 4. The dipolar field value corresponds to the intensity at the magnetic pole. We also

provide an estimate for the characteristic spin-up (positive) or spin-down (negative) timescale. We computed it as the ratio of the total (core plus envelope) angular momentum of the star J_\star and Γ_{ext} obtained with our torque model (see Sect. 2), using the stellar parameters displayed in Table 4.

Using the $Q_{\text{acc}} = 10\%$ model, only AA Tau and BP Tau ($B_{\text{dip}} = 1220$ G) are characterized by a spin-down timescale of a few million years, which is compatible with the Kelvin–Helmholtz contraction timescale. V2129 Oph ($B_{\text{dip}} = 970$ G), BP Tau ($B_{\text{dip}} = 960$ G), CR Cha, and V2247 Oph are in a spin-down state, but the associated timescale is larger than 10 Myr. GQ Lup, V2129 Oph ($B_{\text{dip}} = 280$ G), TW Hya, and CV Cha are in a spin-up state. It is possible to notice that the same object can go from a spin-up to a spin-down state at different epochs, as in the case of V2129 Oph, or conversely, the efficiency of the spin-down torque can change, as is the case of BP Tau, which highlights the usefulness of multi-epoch observations. In applying the $Q_{\text{acc}} = 1\%$ model, only AA Tau would be characterized by a spin-down timescale shorter than 5 Myr.

In our models we also made the limiting assumption that the B_{mod} magnetic field, selected to best reproduce the observed rotational evolution, stays constant during the disk accretion phase. Recently Folsom et al. (2016, 2018) investigated the evolution of the magnetic field strength and topology of low-mass stars from the PMS to the end of MS. They find that up to the

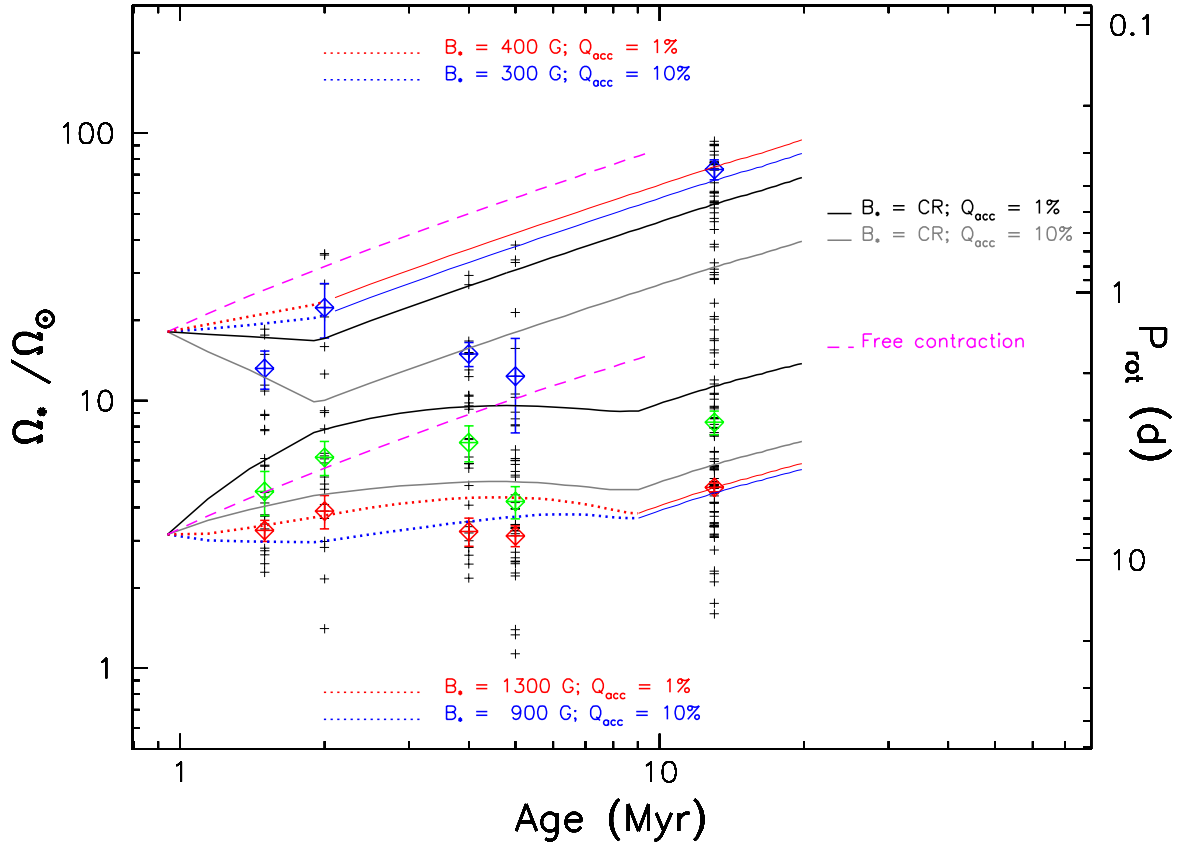


Fig. 5. Same as Fig. 4, but for $\dot{M}_{\text{acc,init}} = 10^{-8} M_{\odot} \text{yr}^{-1}$. It is important to note that for the fast rotation cases, the black and red lines are superimposed.

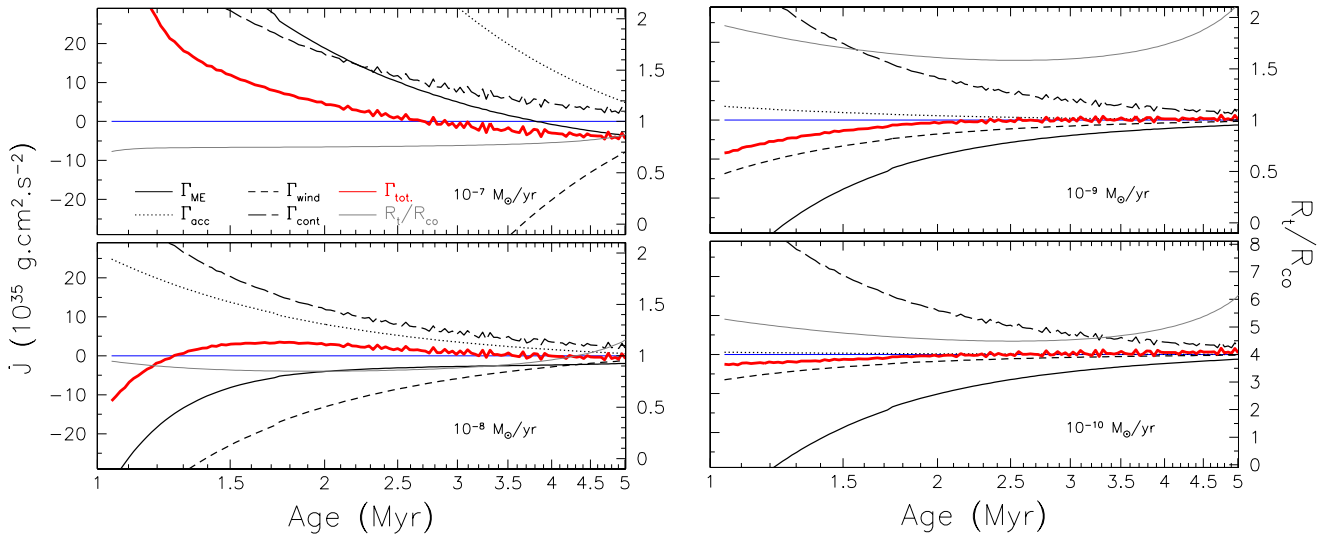


Fig. 6. Evolution of accretion torque Γ_{acc} (dotted line), ME's torque Γ_{ME} (solid line), stellar wind torque Γ_{wind} (short dashed line), and positive torque due to stellar contraction (long dashed line) as function of time for median rotator with $Q_{\text{acc}} = 1\%$ and $\dot{M}_{\text{acc,init}} = 10^{-7} M_{\odot} \text{yr}^{-1}$ (upper panel), $\dot{M}_{\text{acc,init}} = 10^{-8} M_{\odot} \text{yr}^{-1}$ (upper middle panel), $\dot{M}_{\text{acc,init}} = 10^{-9} M_{\odot} \text{yr}^{-1}$ (lower middle panel), and $\dot{M}_{\text{acc,init}} = 10^{-10} M_{\odot} \text{yr}^{-1}$ (lower panel). The red solid line is the sum of all of these torque contributions. The blue solid line represents the zero torque condition leading to a constant angular velocity during the disk accretion phase. The grey solid line shows the evolution of R_t/R_{\odot} .

ZAMS, the magnetic field properties are primarily driven by the structural evolution of the stars, while during the MS phase the magnetic field strength decreases with a decreasing stellar rotational period. Actually, the intensity of the magnetic field rapidly decreases during the first 10 Myr of the stellar evolution (Folsom et al. 2016) following the increase of the complexity of the internal structure (Gregory et al. 2012; Villebrun et al. 2019).

4.2. The interaction regimes

As discussed in Sect. 3.2, the $Q_{\text{acc}} = 10\%$ models, and according to which the mass outflow rate of the stellar wind during the disk accretion phase corresponds to 10% of the mass accretion rate, require a weaker dipolar field that is closer to the typically observed values than the intensities required by the $Q_{\text{acc}} = 1\%$

Table 4. Values of mass accretion rate, dipole magnetic field strength, and stellar radius from [Johnstone et al. \(2014\)](#).

Star	B_{dip} (kG)	M_{\star} (M_{\odot})	R_{\star} (R_{\odot})	$P_{\text{rot},\star}$ (days)	\dot{M}_{acc} ($M_{\odot} \text{ yr}^{-1}$)	$J_{\star}/\Gamma_{\text{ext}}$ (1%/10%; Myr)
V2247 Oph	0.11	0.36	2.00	3.5	1.6×10^{-10}	-503.2/-25.5
CV Cha	0.14	2.0	2.50	4.4	3.2×10^{-8}	0.6/0.7
CR Cha	0.22	1.9	2.50	2.3	1.0×10^{-9}	68.6/-53.4
V2129 Oph 2005	0.28	1.35	2.00	6.53	6.3×10^{-10}	8.1/13.7
TW Hya 2008	0.37	0.8	1.10	3.56	1.3×10^{-9}	2.4/3.1
TW Hya 2010	0.73	0.8	1.10	3.56	1.3×10^{-9}	2.3/3.8
GQ Lup 2011	0.90	1.05	1.70	8.4	1.0×10^{-9}	2.5/5.3
BP Tau Dec 2006	0.96	0.7	1.95	7.6	2.5×10^{-9}	1.6/-14.3
V2129 Oph 2009	0.97	1.35	2.00	6.53	6.3×10^{-10}	17.9/-10.9
GQ Lup 2009	1.07	1.05	1.70	8.4	1.0×10^{-9}	2.6/7.2
BP Tau Feb 2006	1.22	0.7	1.95	7.6	2.5×10^{-9}	2.1/-2.8
AA Tau	1.72	0.7	2.00	8.2	6.3×10^{-10}	-3.5/-1.2

Notes. The stars are sorted by increasing dipole magnetic field strength.

models. On the other hand, the feasibility and nature of these powerful stellar winds is still debated. Since T Tauri stars are slow rotators that spin at a fraction $\leq 10\%$ of their break up speed, stellar winds can not be driven by a magneto-centrifugal mechanism. It is unlikely that the driving force is given by a thermal pressure gradient, which requires a coronal temperature close to virial, that is, $\approx 10^6$ K. [Matt & Pudritz \(2007\)](#) show that a massive wind would have an X-Ray luminosity that is much higher than the typical value observed for T Tauri stars, and its total radiative power would largely exceed the wind kinetic power and even the accretion luminosity. These estimates can provide an upper limit for a thermally-driven wind $\dot{M}_{\text{wind}} \lesssim 10^{-11} M_{\odot} \text{ yr}^{-1}$. In order to cool less efficiently, a more massive wind, such as $\dot{M}_{\text{wind}} \approx 10^{-9} M_{\odot} \text{ yr}^{-1}$, should have a temperature around 10^4 K, and therefore can not be thermally driven. As an alternative, it has been proposed that these winds can be driven by the momentum deposited by Alfvén waves ([Decampli 1981](#)), which are possibly excited and amplified by the impact of the accretion funnels onto the stellar surface (APSW, [Matt & Pudritz 2005a](#)). Moreover, one-dimensional MHD models of this process suggest that the wind mass loss rate can not be higher than 1% of the mass accretion rate ([Cranmer 2008](#)).

On the one hand, if we assume an ejection efficiency of $Q_{\text{acc}} = 1\%$, which is less problematic from the point of view of the stellar wind theory, our models require a stronger dipolar field intensity. Besides, according to our discussion in Sects. 2.3.4 and 3.2, for mass accretion rates lower than approximately $\dot{M}_{\text{acc}} < 10^{-8} M_{\odot} \text{ yr}^{-1}$, which roughly correspond to the maximum spin-down efficiency and to the minima of the B_{mod} values in Table 3 for the $Q_{\text{acc}} = 1\%$ models, the system is likely to enter a “propeller” regime. We recall that a star is in a propeller regime ([Illarionov & Sunyaev 1975](#)) when the inner radius of the accretion disk is equal or larger than the corotation radius (i.e. when $R_{\text{t}} \geq R_{\text{co}}$). In such a situation the spin-down efficiency of the magnetospheric ejections is maximized since they can be directly powered and accelerated by the stellar rotation, and it becomes more important than the torque exerted by the stellar wind.

On the other hand, the centrifugal barrier produced by the stellar rotation makes accretion more difficult since the inner edge of the disk tends to be spun-up by the stellar rotation. Typically, in this regime accretion occurs in cycles ([Romanova et al. 2005, 2018; Lii et al. 2014](#)), which determine a strong variability (no accretion to accretion bursts) and occur on relatively short timescales (a few stellar periods). It is important to notice that this

extreme variability could already occur when the disk is truncated slightly inside the corotation radius. This is due to the fact that as the disk tends to rotate at a sub-Keplerian rate in the truncation region, it can already feel the stellar rotational barrier when $R_{\text{t}} \lesssim R_{\text{co}}$ ([Zanni & Ferreira 2013](#)). As far as we know, this kind of variability has never been observed in CTTS. It must be pointed out that the axisymmetric MHD simulations commonly used to investigate the propeller regime could strongly amplify this effect. As a matter of fact, AA Tau, which we recall being the only star in Table 4 to be efficiently spun-down when applying our $Q_{\text{acc}} = 1\%$ model, should be truncated very close to the corotation radius, but this star has never shown the variability usually found in propeller models. Both conditions are theoretically (the mass carried by stellar wind i.e. $Q_{\text{acc}} = 10\%$) and observationally (the strong variability introduced by the propeller regime) problematic.

4.3. Early-PMS rotation rate

Since the results of the models are compared to the observations, the cluster’s age is a key parameter. Unfortunately, the age of PMS clusters is poorly constrained yet ([Bell et al. 2013](#)) this factor limits the strength of the results presented here. The uncertainties in the rotation period measurement induced by, for example, synchronized binaries and multiple spots at the stellar surface ([Bouvier et al. 1997; Moraux et al. 2013](#)) are in principle already included in the error bars given by the rejection method used in this study (see [Gallet & Bouvier 2013, 2015](#)). Moreover, the age estimations come from different observations, methods, and techniques that thus provide an inhomogeneous temporal sample. This highlights the need for a self-consistent analysis of clusters properties.

Besides this age estimation limitation, there are several observational biases in terms of rotation period measurement. These measurements are usually realized by extracting quasi-periodic modulations in the photometric observation of a given star that is induced by the presence of surface stellar spots. Hence, the nature of the technique itself leads to observations that are more sensitive to magnetically active fast rotating stars, for which several complete rotational periods can be monitored during the observation time.

We can also mention that the metallicity could have a strong effect on the rotational evolution of low-mass stars, even during their early-PMS phase evolution. Indeed, changing the

initial metal content of a star can mimic the effect of changing its initial mass on the evolution of the stellar internal structure. A decrease of metallicity induces a reduction of the global opacity of the star that allows for an easier redistribution of the energy inside of the convective envelope and thus leads to an increase of the stellar surface effective temperature (see [Amard et al. 2019](#)).

4.4. Observational evidences of magnetospheric outflows

Outflows from the innermost parts of the star-disk interaction region play a fundamental role for the stellar spin evolution in our framework. They have been typically associated with the blue-shifted components either in the emission of forbidden lines, or in the absorption of permitted ones.

For example the P-Cygni profile of the He I $\lambda 10830$ line has proven to be a sensible diagnostic for both infall and outflow ([Dupree et al. 2005](#); [Edwards et al. 2006](#)). In particular [Edwards et al. \(2006\)](#) propose that broad and deep blue-shifted absorption features could be associated with a stellar wind in systems seen at low inclinations, as in the TW Hya case ([Dupree et al. 2014](#)). Radiative transfer calculations have confirmed this hypothesis but, at least in the specific case of AS 353 A, a massive ($\dot{M}_{\text{wind}} > 10^{-9} M_{\odot} \text{yr}^{-1}$) and relatively cold (8000 K) wind is required to reproduce the observations ([Kurosawa et al. 2011](#)). These estimates raise questions about the nature of these putative stellar winds, as previously mentioned in Sect. 4.2.

On the other hand, [Edwards et al. \(2006\)](#) associate narrow blue-shifted absorption features of the He I $\lambda 10830$ line with outflows emerging from the inner disk of systems seen at high inclinations. In the case of AA Tau, a prototypical CTTS seen at high inclination, [Bouvier et al. \(2003\)](#) observed a correlation between the variations of the radial velocity of the blue-shifted (outflow) and red-shifted (inflow) absorption components in the H α line profile. The authors interpret this correlation to be due to a periodic inflation and reconnection of the stellar magnetic field. This interpretation is qualitatively consistent with the behaviour of magnetospheric ejections, but the variability that the numerical models of [Zanni & Ferreira \(2013\)](#) require to efficiently slow down the stellar rotation is much more extreme than the one displayed, for example, by AA Tau. In general, young stellar objects are known to be characterized by accretion and ejection outbursts (see e.g. [Ansdell et al. 2016](#)) but, as far as we know, this burst-like behaviour has never been observed on the relatively short timescales (a few stellar periods) that seem to characterize the simulations of the propeller regime.

In any case, it is not clear whether it is possible or not to use the blueshifted absorption components to differentiate between the possible inner disk outflow scenarios, that is, MEs, an X-wind, an ReX-wind, or the inner part of a more extended disk-wind. For example the radiative transfer calculations of [Kurosawa et al. \(2011\)](#) and [Kurosawa & Romanova \(2012\)](#) that are based on a semi-analytic toy model of a more extended disk-wind and a numerical MHD model of a conical wind solution (that we think to be closely related to the MEs), respectively, provide qualitatively the same line profiles. More detailed radiative transfer calculations of different outflow classes are required to attempt a more quantitative comparison with observations and constrain the properties of these winds and their possible influence on the stellar spin evolution.

5. Summary and conclusions

Different measurements of the rotational period distribution of young star-forming regions lead to the conclusion that the

surface rotation rate of stars remains approximately constant during their early-PMS phase. This stage seems to be related to the epoch during which the forming stars are still surrounded by, and interact with, an accretion disk. These observations hence have motivated angular momentum evolution models to often simply consider a constant surface angular velocity during the first few Myr of the stellar life so as to mimic this observed feature ([Gallet & Bouvier 2013, 2015](#); [Amard et al. 2016](#)).

To improve this simplified vision of a constant surface rotation rate, we decided to include an actual star-disk interaction model in our angular momentum evolution calculations so as to investigate what properties of CTTS are required to fulfill the observations constraints. In this study, we directly compared the angular velocity evolution that results from our star-disk interaction model to rotation period observations of solar-type stars.

We pointed out that a kG dipolar magnetic field component is typically required during the entire disk lifetime so as to extract enough angular momentum from the stellar surface to compensate for the acceleration of the stars due to their contraction and accretion. While such strong dipolar magnetic field intensity is sometimes detected, it is not ubiquitous. Indeed, at the very beginning of their evolution, young and fully convective CTTS (e.g. AA Tau and BP Tau) are sometimes observed to display strong dipolar magnetic field components between 1 kG and 2 kG. This dipolar magnetic field intensity is then ideal for rotational regulation through star-disk magnetic interaction processes.

Besides, we find that, to have an efficient spin-down, the interaction regimes are often rather extreme. Our models frequently require either of the following: firstly, strong stellar winds, with a mass loss rate around 10% of the accretion rate, that seem hard to produce due to general energetic considerations; or secondly, being in a propeller regime ($R_{\text{t}} > R_{\text{co}}$) that maximizes the spin-down efficiency of magnetospheric ejections, but at least according to axisymmetric numerical models, triggers an extreme accretion variability that is generally not observed.

The results of this work should, however, be considered as preliminary and a more physical model has yet to be developed. More specifically, we should investigate star-disk interaction models in which the impact of a non-axisymmetric and multipolar magnetic field is taken into account, or include other effects that could influence the spin evolution, such as the accretion and ejection bursts associated with FU Ori events that are neglected in this work.

Acknowledgements. We thank the anonymous referee for the constructive comments about our work that increased the quality of the paper. F.G. acknowledges financial support from the CNES fellowship. This study was supported by the grant ANR 2011 Blanc SIMI5-6 020 01 “Toupies: Towards understanding the spin evolution of stars” (http://ipag.osug.fr/Anr_Toupies/). We acknowledge financial support from CNRS-INSU’s Programme National de Physique Stellaire. This project has received funding from the European Research Council (ERC) under the European Union’s Horizon 2020 research and innovation program (grant agreement No 742095; *SPIDI*: Star-Planets-Inner Disk-Interactions). F.G. acknowledges financial support from the CNES fellowship. LA gratefully acknowledges financial support from the ERC (grant 682393, *AWESoMe Stars*). We thank C. Johnstone for enlightening discussions on CTTS magnetic field evolution.

References

- Allain, S. 1998, *A&A*, 333, 629
 Amard, L., Palacios, A., Charbonnel, C., Gallet, F., & Bouvier, J. 2016, *A&A*, 587, A105
 Amard, L., Palacios, A., Charbonnel, C., et al. 2019, *A&A*, 631, A77
 Ansdell, M., Gaidos, E., Rappaport, S. A., et al. 2016, *ApJ*, 816, 69

- Armitage, P. J., & Clarke, C. J. 1996, *MNRAS*, **280**, 458
- Asplund, M., Grevesse, N., Sauval, A. J., & Scott, P. 2009, *ARA&A*, **47**, 481
- Bell, C. P. M., Naylor, T., Mayne, N. J., Jeffries, R. D., & Littlefair, S. P. 2013, *MNRAS*, **434**, 806
- Bessolaz, N., Zanni, C., Ferreira, J., Keppens, R., & Bouvier, J. 2008, *A&A*, **478**, 155
- Bouvier, J., Cabrit, S., Fernandez, M., Martin, E. L., & Matthews, J. M. 1993, *A&A*, **272**, 176
- Bouvier, J., Forestini, M., & Allain, S. 1997, *A&A*, **326**, 1023
- Bouvier, J., Grankin, K. N., Alencar, S. H. P., et al. 2003, *A&A*, **409**, 169
- Bouvier, J., Matt, S. P., Mohanty, S., et al. 2014, *Protostars Planets VI*, 433
- Caratti O Garatti, A., Garcia Lopez, R., Antonucci, S., et al. 2012, *A&A*, **538**, A64
- Collier Cameron, A., & Campbell, C. G. 1993, *A&A*, **274**, 309
- Collier Cameron, A., Campbell, C. G., & Quaintrell, H. 1995, *A&A*, **298**, 133
- Cranmer, S. R. 2008, *ApJ*, **689**, 316
- Cranmer, S. R., & Saar, S. H. 2011, *ApJ*, **741**, 54
- Decampli, W. M. 1981, *ApJ*, **244**, 124
- Donati, J. F., Bouvier, J., Walter, F. M., et al. 2011, *MNRAS*, **412**, 2454
- Dupree, A. K., Brickhouse, N. S., Smith, G. H., & Strader, J. 2005, *ApJ*, **625**, L131
- Dupree, A. K., Brickhouse, N. S., Cranmer, S. R., et al. 2014, *ApJ*, **789**, 27
- Edwards, S., Strom, S. E., Hartigan, P., et al. 1993, *AJ*, **106**, 372
- Edwards, S., Hartigan, P., Ghandour, L., & Andriulis, C. 1994, *AJ*, **108**, 1056
- Edwards, S., Fischer, W., Hillenbrand, L., & Kwan, J. 2006, *ApJ*, **646**, 319
- Ferreira, J., Pelletier, G., & Appl, S. 2000, *MNRAS*, **312**, 387
- Finley, A. J., & Matt, S. P. 2018, *ApJ*, **854**, 78
- Folsom, C. P., Petit, P., Bouvier, J., et al. 2016, *MNRAS*, **457**, 580
- Folsom, C. P., Bouvier, J., Petit, P., et al. 2018, *MNRAS*, **474**, 4956
- Gallet, F., & Bouvier, J. 2013, *A&A*, **556**, A36
- Gallet, F., & Bouvier, J. 2015, *A&A*, **577**, A98
- Ghosh, P., & Lamb, F. K. 1979, *ApJ*, **234**, 296
- Gregory, S. G., Donati, J.-F., Morin, J., et al. 2012, *ApJ*, **755**, 97
- Hartmann, L., Calvet, N., Gullbring, E., & D'Alessio, P. 1998, *ApJ*, **495**, 385
- Henderson, C. B., & Stassun, K. G. 2012, *ApJ*, **747**, 51
- Illarionov, A. F., & Sunyaev, R. A. 1975, *A&A*, **39**, 185
- Irwin, J., & Bouvier, J. 2009, in *IAU Symp.*, eds. E. E. Mamajek, D. R. Soderblom, & R. F. G. Wyse, 258, 363
- Irwin, J., Hodgkin, S., Aigrain, S., et al. 2008, *MNRAS*, **384**, 675
- Johns-Krull, C. M. 2007, *ApJ*, **664**, 975
- Johns-Krull, C. M., Greene, T. P., Doppmann, G. W., & Covey, K. R. 2009, *ApJ*, **700**, 1440
- Johnstone, C. P., Jardine, M., Gregory, S. G., Donati, J.-F., & Hussain, G. 2014, *MNRAS*, **437**, 3202
- Johnstone, C. P., Güdel, M., Lüftinger, T., Toth, G., & Brott, I. 2015, *A&A*, **577**, A27
- Königl, A. 1991, *ApJ*, **370**, L39
- Kurosawa, R., & Romanova, M. M. 2012, *MNRAS*, **426**, 2901
- Kurosawa, R., Romanova, M. M., & Harries, T. J. 2011, *MNRAS*, **416**, 2623
- Lii, P. S., Romanova, M. M., Ustyugova, G. V., Koldoba, A. V., & Lovelace, R. V. E. 2014, *MNRAS*, **441**, 86
- Littlefair, S. P., Naylor, T., Mayne, N. J., Saunders, E. S., & Jeffries, R. D. 2010, *MNRAS*, **403**, 545
- Livio, M., & Pringle, J. E. 1992, *MNRAS*, **259**, 23P
- Long, M., Romanova, M. M., & Lovelace, R. V. E. 2005, *ApJ*, **634**, 1214
- MacGregor, K. B., & Brenner, M. 1991, *ApJ*, **376**, 204
- Matt, S., & Pudritz, R. E. 2005a, *ApJ*, **632**, L135
- Matt, S., & Pudritz, R. E. 2005b, *MNRAS*, **356**, 167
- Matt, S., & Pudritz, R. E. 2007, in *Star-Disk Interaction in Young Stars*, eds. J. Bouvier, & I. Appenzeller, *IAU Symp.*, **243**, 299
- Matt, S., & Pudritz, R. E. 2008, *ApJ*, **678**, 1109
- Matt, S. P., Pinzón, G., de la Reza, R., & Greene, T. P. 2010, *ApJ*, **714**, 989
- Matt, S. P., MacGregor, K. B., Pinsonneault, M. H., & Greene, T. P. 2012, *ApJ*, **754**, L26
- Matt, S. P., Brun, A. S., Baraffe, I., Bouvier, J., & Chabrier, G. 2015, *ApJ*, **799**, L23
- Morau, E., Artemenko, S., Bouvier, J., et al. 2013, *A&A*, **560**, A13
- Morin, J., Donati, J.-F., Petit, P., et al. 2008, *MNRAS*, **390**, 567
- Morin, J., Donati, J.-F., Petit, P., et al. 2010, *MNRAS*, **407**, 2269
- Oglethorpe, R. L. F., & Garaud, P. 2013, *ApJ*, **778**, 166
- Pantolmos, G., & Matt, S. P. 2017, *ApJ*, **849**, 83
- Rebull, L. M., Wolff, S. C., & Strom, S. E. 2004, *AJ*, **127**, 1029
- Réville, V., Brun, A. S., Strugarek, A., et al. 2015, *ApJ*, **814**, 99
- Rodríguez-Ledesma, M. V., Mundt, R., & Eisloffel, J. 2009, *A&A*, **502**, 883
- Romanova, M. M., Ustyugova, G. V., Koldoba, A. V., & Lovelace, R. V. E. 2005, *ApJ*, **635**, L165
- Romanova, M. M., Ustyugova, G. V., Koldoba, A. V., & Lovelace, R. V. E. 2009, *MNRAS*, **399**, 1802
- Romanova, M. M., Blinova, A. A., Ustyugova, G. V., Koldoba, A. V., & Lovelace, R. V. E. 2018, *New A*, **62**, 94
- See, V., Jardine, M., Vidotto, A. A., et al. 2018, *MNRAS*, **474**, 536
- Shu, F., Najita, J., Ostriker, E., et al. 1994, *ApJ*, **429**, 781
- Villebrun, F., Alecian, E., Hussain, G., et al. 2019, *A&A*, **622**, A72
- Weber, E. J., & Davis, Jr., L. 1967, *ApJ*, **148**, 217
- Wright, N. J., Drake, J. J., Mamajek, E. E., & Henry, G. W. 2011, *ApJ*, **743**, 48
- Zanni, C., & Ferreira, J. 2009, *A&A*, **508**, 1117
- Zanni, C., & Ferreira, J. 2013, *A&A*, **550**, A99